Dovepress

ORIGINAL RESEARCH

Qingfei Huoxue Decoction and Its Active Component Narirutin Alleviate LPS-Induced Acute Lung Injury by Regulating TLR4/NF-κB Pathway Mediated Inflammation

Yule Wang*, Bei Li*, Yingjuan Zhang*, Ruiling Lu, Qianzhuo Wang, Yue Gao

Zhejiang Key Laboratory of Traditional Chinese Medicine for the Prevention and Treatment of Senile Chronic Diseases, Department of Geriatrics, Affiliated Hangzhou First People's Hospital, School of Medicine, Westlake University, Hangzhou, People's Republic of China

*These authors contributed equally to this work

Correspondence: Yue Gao, Zhejiang Key Laboratory of Traditional Chinese Medicine for the Prevention and Treatment of Senile Chronic Diseases, Department of Geriatrics, Affiliated Hangzhou First People's Hospital, School of Medicine, Westlake University, 261 huansha Road, Shangcheng District, Hangzhou, 310006, People's Republic of China, Email gaoyue@hospital.westlake.edu.cn

Background: Acute lung injury (ALI) is a life-threatening clinical syndrome with high mortality. Currently, the safe and effective therapies for ALI patients are still limited. Qingfei Huoxue decoction (QFHXD) is a hospital agreement prescription for treating pulmonary diseases and displays a remarkable efficacy. However, the pharmacological effect of QFHXD on preventing lipopolysaccharide (LPS)-induced ALI has yet to be reported, let alone questions of potential molecular mechanisms and anti-ALI active substances.

Methods: To answer the above-mentioned questions, histopathological observation and kit detection were performed to estimate the protective effect of QFHXD pretreatment against LPS-induced ALI. Based on comprehensive chemical profiling of QFHXD, a network pharmacology strategy and experimental validation were integrated to elucidate the underlying functional mechanisms. The potential anti-ALI active components were identified by molecular docking. The anti-ALI activity of narirutin and its anti-inflammatory mechanism were further validated using animal and molecular experiments.

Results: Pretreatment with different doses of QFHXD effectively mitigated histopathological lesions and systemic inflammation caused by LPS stimulation. A detailed analysis of established compound-target-disease network revealed the strong correlation between anti-ALI action of QFHXD and inflammatory mechanisms. Compared with the model group, QFHXD intervention markedly restrained the abnormally increased transcription and protein levels of pro-inflammatory factors (TLR4, NF-κB, IL-6, IL-1β, and TNF-α) in lung tissues of ALI mice. The results of molecular docking highlighted the anti-ALI potential of narirutin targeting to TLR4 and NF-κB p65. In addition to the protective effect of narirutin on suppressing LPS-induced pathological changes, we found that narirutin pretreatment effectively normalized the disordered protein levels of above pro-inflammatory factors of ALI mice.

Conclusion: These interesting findings indicate the beneficial effects of QFHXD and its active component narirutin against ALI partly via regulating TLR4/NF-κB mediated inflammation. This work contributes to the development of novel medications for ALI patients.

Keywords: Qingfei Huoxue decoction, narirutin, LPS-induced acute lung injury, network pharmacology, TLR4/NF-κB pathway, inflammatory response

Introduction

Acute lung injury (ALI) and its more severe form, acute respiratory distress syndrome (ARDS), are the leading causes of acute respiratory failure in critically ill patients with high morbidity and poor clinical outcomes.[1] Especially, with the outbreak of the Coronavirus Disease 2019 (COVID-19), ALI/ARDS significantly contributes to the mortality in patients

7503

Graphical Abstract
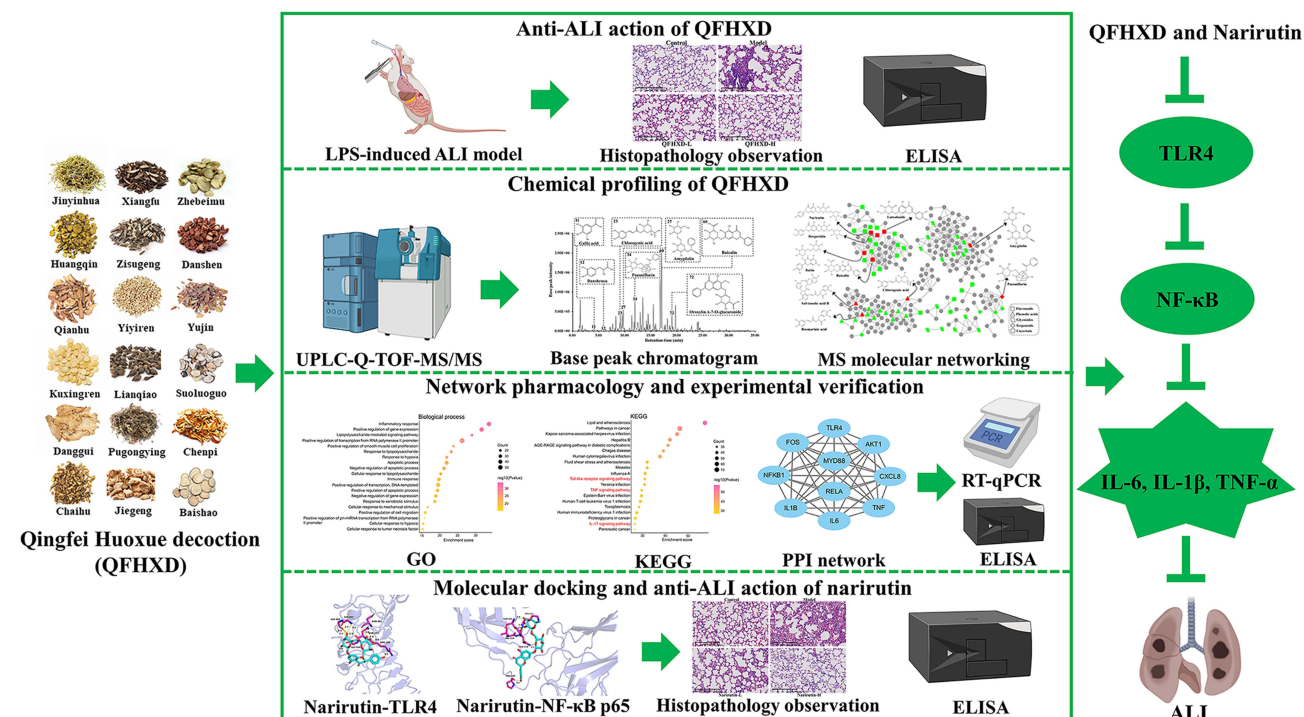
with COVID-19.[2] As a major clinical problem worldwide, a variety of pulmonary and extra-pulmonary triggers accelerate the onset of ALI, such as pneumonia, pulmonary contusion, non-pulmonary sepsis, severe trauma with shock, and transfusion-related ALI.[3] The pathological characteristics of ALI are mainly manifested by diffuse alveolar damage with dysfunction of alveolar epithelial-capillary endothelial barrier, pulmonary edema, local inflammatory accumulation (activation of immune cells and production of pro-inflammatory mediators), eventually resulting in severe lung consolidation.[1,4] To date, apart from the recommended non-pharmacological intervention (lung-protective mechanical ventilation), corticosteroids, phosphodiesterase inhibitors, and neuromuscular blockers appear to be the most promising medications.[5,6] However, the limited options and medical burden urgently call for the novel therapeutic approaches.

In China, Chinese medicines (CMs) have a long history in the clinical practice of ALI.[7] From the perspective of traditional Chinese medicine (TCM), the main pathogenesis of ALI can be summarized as heat, toxin, phlegm, and stasis, and the TCM prescriptions with the functions of clearing heat and detoxifying as well as expelling phlegm and removing blood stasis should be used.[8] As a hospital agreement prescription, Qingfei Huoxue decoction (QFHXD), which comprises *Lonicera japonica* Thunb. (Jinyinhua), *Scutellaria baicalensis* Georgi (Huangqin), *Peucedanum praeruptorum* Dunn (Qianhu), *Prunus mandshurica* (Maxim.) Koehne (Kuxingren), *Angelica sinensis* (Oliv.) Diels (Danggui), *Bupleurum chinense* DC. (Chaihu), *Cyperus rotundus* L. (Xiangfu), *Perilla frutescens* (L.) Britton (Zisugeng), *Coix lacryma-jobi var. ma-yuen* (Rom. Caill). Stapf (Yiyiren), *Forsythia suspensa* (Thunb.) Vahl (Lianqiao), *Taraxacum mongolicum* Hand.-Mazz. (Pugongying), *Platycodon grandiflorus* (Jacq). A. DC. (Jiegeng), *Fritillaria thunbergii* Miq. (Zhebeimu), *Salvia miltiorrhiza* Bunge (Danshen), *Curcuma wenyujin* Y.H.Chen & C.Ling (Yujin), *Aesculus chinensis* Bunge (Suoluoguo), *Citrus reticulata* Blanco (Chenpi), and *Paeonia lactiflora* Pall. (Baishao), has been frequently prescribed for the treatment of pulmonary diseases with TCM syndrome of lung heat, phlegm coagulation, *Qi* stagnation, and blood stasis, and has a definite curative effect.

The growing preclinical and clinical studies suggest that inflammation is strongly linked to the progress of ALI.[9–11] For example, excessive activation and migration of neutrophils exacerbate the release of pro-inflammatory mediators, especially neutrophil extracellular traps (NETs).[12] Overproduction of NETs can promote the polarization of alveolar macrophages to pro-inflammatory phenotype and aggravate lung injury.[13] The hyper-inflammatory phenotype, covering approximately one-third of ARDS patients, is associated with higher levels of circulating cytokines and increased mortality.[4] Currently, anti-inflammatory therapies are believed to contribute to better clinical outcomes in ALI/ARDS patients with hyper-inflammatory phenotype.[14] As representative CMs for heat-clearing and toxin-resolving, Jinyinhua, Pugongying, Lianqiao, and Huangqin were observed to mitigate ALI via anti-inflammatory pathways.[15–18] The CMs for expelling phlegm (eg, Jiegeng and Zhebeimu) as well as the CMs for promoting *Qi* (eg, Xiangfu, Chaihu, and Chenpi) could also inhibit inflammation to exert anti-ALI effects.[19–23] With the functions of invigorating blood circulation and removing stasis, Danshen and Danggui were found to lighten ALI via inhibiting inflammation and apoptosis.[24–26] Based on the above mentioned anti-ALI activities of main CMs of QFHXD, QFHXD may possess a great potential against ALI. However, the pharmacological action, possible molecular mechanisms, and active substances of QFHXD against ALI remain indistinct and deserve further investigation.

In this research, the efficacy of QFHXD against ALI was evaluated in a lipopolysaccharide (LPS)-stimulated mouse model. Referring to a previous report,[27] the comprehensive chemical characterization of QFHXD was performed via integration of ultra-high-performance liquid chromatography combined with quadrupole time-of-flight tandem mass spectrometry (UPLC-Q-TOF-MS/MS) and mass spectrometry molecular networking (MSMN). Based on the definitely identified main compounds in QFHXD, the network was plotted to systematically probe the possible functional mechanisms of QFHXD against ALI followed by experimental verification. To determine the anti-ALI active constituents, molecular docking of protein receptors and compound ligands was executed. The active ingredients with anti-ALI potential were further validated in animal and molecular experiments. The findings of current study are expected to provide data support for further clinical application of QFHXD and offer an alternative pharmacotherapy for ALI patients.

Materials and Methods
Drugs and Reagents
QFHXD (Supplementary Table S1) was prepared by Zhejiang Key Laboratory of Traditional Chinese Medicine for the Prevention and Treatment of Senile Chronic Diseases. TCM decoction pieces, obtained from TCM pharmacy of Hangzhou First People's Hospital, were mixed, soaked, and decocted thrice for 60 min each time. The decoction was freeze-dried into powder under vacuum condition. LPS from *Escherichia coli* (O111:B4) (L2630), dimethyl sulfoxide (DMSO, 276855), and 2, 2, 2-Tribromoethanol (T48402) were obtained from Sigma-Aldrich. Adenosine (B21356), gallic acid (B20851), loganic acid (B20823), epicatechin (B20102), rutin (B20771), luteoloside (B20887), and baicalin (B20570) were purchased from Yuanye Biotechnology Co., Ltd. (Shanghai, China). Danshensu (DD0015), (+)-catechin (DE0001), paeoniflorin (DS0070), salvianolic acid A (DD0008), and salvianolic acid B (DD0009) were purchased from DESITE Biotechnology Co., Ltd. (Chengdu, China). Chlorogenic acid (A0022), narirutin (A0132), and hesperidin (A0032) were purchased from MUST Biotechnology Co., Ltd. (Chengdu, China). Amygdalin (TFL085), rosmarinic acid (TBB012), and Oroxylin A-7-O-glucuronide (THT042) were purchased from WINHERB Pharmaceutical Technology Development Co., Ltd. (Shanghai, China). The purities of above standards were no less than 98%. Paraformaldehyde fix solution (4%, E672002) was provided by Sangon Biotechnology Co., Ltd. (Shanghai, China). Ultra-pure water was prepared using a Millipore-Q water purification system (Millipore, Milford, MA, USA). Chromatographic-grade methanol (22035147) and acetonitrile (22055247) were obtained from TEDIA. Formic acid (P1881926) was obtained from Titan Technology Co., Ltd. (Shanghai, China). Hematoxylin & Eosin (H&E) staining kit (C0105S) was purchased from Beyotime Biotechnology Co., Ltd. (Shanghai, China). TriZol reagent (CW0580S) was bought from CoWin Biotechnology Co., Ltd. (Beijing, China). 5×Easy RT Master Mix (-DNase) (PR0403100) was bought from Easy-Do Biotechnology Co., Ltd. (Hangzhou, China). ChamQ SYBR qPCR Master Mix (Q321-02) was bought from Vazyme Biotechnology Co., Ltd. (Nanjing, China). Mouse TLR4 (ZC-37841), NF-κB (ZC-39080), IL-6 (ZC-37988), IL-1β (ZC-37974), and TNF-α (ZC-39024) ELISA kits were obtained from ZCi Biotechnology Co., Ltd. (Shanghai, China).

Sample Preparation

QFHXD freeze-dried powder (10 mg) was accurately weighed and dissolved with 1 mL ultra-pure water. After accurately weighing, all the standards were mixed and dissolved in 1 mL of 50% methanol. Following centrifuging at 13,000 rpm for 10 min, the supernatants of QFHXD sample and mixed standards were, respectively, collected for further analysis.

UPLC-Q-TOF-MS/MS Analysis

An ACQUITY UPLC system (Waters, Milford, MA, USA) coupled with a Triple TOF 6600 plus MS (AB SCIEX, Framingham, MA, USA) was utilized for chemical detection of QFHXD sample. The chromatographic separation was carried out using the Waters ACQUITY UPLC HSS T3 column (2.1 × 150 mm, 1.8 μm, Waters Corp.) and the column temperature was maintained at 50 °C. The mobile phases consisted of 0.1% formic acid-water (A) and 0.1% formic acid-acetonitrile (B) and the flow rate was maintained at 0.3 mL/min. The injection volume was 3 μL, and a linear gradient elution was programmed as follows: 0 min, 2% B; 2 min, 5% B; 20 min, 35% B; 30 min, 95% B, 32 min, 95% B, 35 min, 2% B. Mass spectrometry analysis was performed in both positive electrospray ionization (ESI$^+$) and negative electrospray ionization (ESI$^-$) modes with the following main parameters: scan range, m/z 100–1500; ion source GS1, 55 psi; ion source GS2, 55 psi; curation gas (CUR), 35 psi; ion source temperature, 600 °C for ESI$^+$ and 550 °C for ESI$^-$; ion source voltage, 5.5 kV for ESI$^+$ and −4.5 kV for ESI$^-$; declustering potential (DP), 100 V; collision energy (CE), 10 V. MS^2 data were collected in information-dependent acquisition (IDA) mode.

Construction of Mass Spectrometry Molecular Network

The online workflow at Global Natural Products Social Molecular Networking (GNPS, http://gnps.ucsd.edu) was employed to construct the MS/MS-based molecular network.[27,28] Raw mass spectral data were converted to .mzML format using MSConvert software (ProteoWizard, http://proteowizard.sourceforge.net) and then uploaded to GNPS to generate the molecular network. Both the precursor ion mass tolerance and the fragment ion mass tolerance were set to 0.02 Da. The network top-k of 10, minimum cluster size of 2, maximum connected component size of 100, maximum shift of 500 Da, and minimum matched fragment ions of 5 were set. The network was constructed with the minimum 5 matched peaks and a cosine score above 0.7. The spectral libraries on GNPS were applied for retrieval and comparison. The results were visualized with Cytoscape 3.7.2.

Experimental Animals

Eight-week-old adult male C57BL/6J mice (20–22 g) were obtained from Shanghai SLAC Laboratory Animal Co., Ltd. (Shanghai, China, Certificate No.: SCXK [Hu] 2017–0005). All animal studies were performed following the guidance of the Care and Use of Laboratory Animals published by the US National Institutes of Health (NIH Publication No.85–23, revised 1996) and the protocols of animal experiments were approved by the Laboratory Animal Welfare and Ethics Committee of Zhejiang Center of Laboratory Animals (Approval number: ZJCLA-IACUC-20010494). The mice were housed in an air-conditioned room with the temperature of 25 ± 1 °C, relative humidity of 45 ± 5%, and a 12-h light/dark cycle. The mice were allowed to freely access to standard rodent chow and clean water.

Animal Grouping and Drug Intervention

Forty mice were randomly divided into control, model (LPS), QFHXD low dose (QFHXD-L, 4.78 g/kg), and QFHXD high dose (QFHXD-H, 9.56 g/kg) groups. The dosage of QFHXD-L used in mice was converted from clinical dosage with the following formula: The dosage of QFHXD-L = 213 g × 14.8% × 9.1/60 kg (the clinical dosage for adult was 213 g/person/day, the extractum yield rate was 14.8%, the equivalent-dose ratio of human and mouse was 9.1, and the average weight of adults was 60 kg). Seven days before LPS modeling, the mice were continuously administered different doses of QFHXD via gavage for once daily. The control and model groups received intragastric administration of ultrapure water at a dose of 10 mL/kg. For narirutin, forty mice were randomly divided into control group, model (LPS) group, narirutin low dose (narirutin-L, 20 mg/kg) group, narirutin high dose (narirutin-H, 40 mg/kg) group. The mice in drug intervention groups were intraperitoneally injected with different doses of narirutin dissolved in ultrapure

water containing 1% DMSO once daily for seven days. The control and model groups were pretreated with ultrapure water containing 1% DMSO at a dose of 10 mL/kg via intraperitoneal administration.

LPS-Induced ALI Model

On the 8th day, a LPS-induced ALI mouse model was established. Briefly, 30 min after the last dose, the experimental animals were anesthetized. Subsequently, LPS at a dose of 5 mg/kg was injected through endotracheal intubation. An equal volume of normal saline was administered to control mice.

Histopathology Observation

Twenty-four hours after LPS modeling, the lung tissues (n = 4 for each group) were collected. After fixation for at least 48 h, the tissues were dehydrated, embedded, and sliced. After treatment with H&E staining solution, an automatic digital slide scanning system (KF-PRO-120, KFBIO, China) was applied for the acquisition of histopathological images. The histo-pathology observation was performed with 200X magnification using the KFBIO digital slide viewer (Version 1.7.0.21).

Data Mining of Main Compounds Related Targets

After the identification of major compounds in QFHXD, a high-throughput experiment- and reference-guided database of traditional Chinese medicine (HERB) (http://herb.ac.cn/), Traditional Chinese Medicine Systems Pharmacology Database and Analysis Platform (TCMSP) (http://old.tcmsp-e.com/tcmsp.php/), and PubMed (http://www.ncbi.nlm.nih.gov/pubmed/) were united to gather potential targets of main compounds.[29,30] The representative compound-target network was visualized using R (Version 4.0.2, http://www.r-project.org/).

Collection of ALI Related Targets

The online databases, including GeneCards (http://www.genecards.org/), DisGeNET (http://www.disgenet.org/), and Phenopedia (https://phgkb.cdc.gov/), were retrieved to collect the genes relevant to ALI.[31–33] Among them, the genes with Relevance Score greater than 20 in GeneCards were selected.

Network Construction and Analysis

The overlapped targets between disease-target network and compound-target network were recognized using an online tool named Bioinformatics & Evolutionary Genomics (http://bioinformatics.psb.ugent.be/webtools/Venn/) and the Venn diagram was automatically generated. To further explore the possible mechanisms of QFHXD in alleviating ALI, the list of overlapped genes was imported into the online Database for Annotation, Visualization and Integration Discovery (DAVID) bioinformatics tool (Version 6.8, http://david.ncifcrf.gov/) to execute the Gene Ontology (GO) and Kyoto Encyclopedia of Genes and Genomes (KEGG) enrichment analyses.[34] An easy-to-use data visualization web server named ImageGP was employed for the visualization of top biological processes and signaling pathways.[35]

Construction and Analysis of Protein–Protein Interaction (PPI) Network

The data of PPI network of overlapped genes were acquired using the Search Tool for Recurring Instances of Neighboring Genes (STRING) database (http://string-db.org/) followed by subsequent visualization and detailed analysis using Cytoscape software (Version 3.7.2). The plug-in of Molecular Complex Detection (MCODE) in Cytoscape software was employed to determine the most critical subnetwork.[36] To screen the top nodes from PPI cluster, we operated the plug-in of cytoHubba based on the topological analysis methods of Degree and density of maximum neighborhood component (DMNC).[37] Through the aggregation of top nodes ranked by cytoHubba as well as the genes participated in the significant molecular mechanisms, the PPI network of hub genes for follow-up experimental verification was presented.

Real-Time Quantitative Polymerase Chain Reaction (RT-qPCR) Analysis

Total RNA of lung tissues (n = 5 for each group) was extracted using the TRIzol method. Following reverse transcription, the mRNA levels of hub genes were measured using the SYBR Green I fluorescence method. The $2^{-\Delta\Delta CT}$ method was

applied to calculate the relative mRNA expression levels of target genes with glyceraldehyde 3-phosphate dehydrogenase (GAPDH) as normalization. The details of primer sequences were described as follow: for TLR4 forward 5′-ATG GCA TGG CTT ACA CCA CC-3′, reverse 5′-GAG GCC AAT TTT GTC TCC ACA-3′; for NF-κB p65 forward 5′-AGG CTT CTG GGC CTT ATG TG-3′, reverse 5′-TGC TTC TCT CGC CAG GAA TAC-3′; for IL-6 forward 5′-TAG TCC TTC CTA CCC CAA TTT CC-3′, reverse 5′-TTG GTC CTT AGC CAC TCC TTC-3′; for IL-1β forward 5′-AGG CTG ACA GAC CCC AAA AG-3′, reverse 5′-CTC CAC GGG CAA GAC ATA GG-3′; for TNF-α forward 5′-CCC TCA CAC TCA GAT CAT CTT CT-3′, reverse 5′-GCT ACG ACG TGG GCT ACA G-3′; for GAPDH forward 5′-TGG TGA AGC AGG CAT CTG AG-3′, reverse 5′-TGC TGT TGA AGT CGC AGG AG-3′.

Enzyme-Linked Immunosorbent Assay (ELISA)

Twenty-four hours after LPS modeling, the blood samples (n = 6 for each group) were collected from anesthetized mice, and then the serum was separated by centrifugation at 3500 rpm for 15 min at 4 °C. After euthanizing the mice, the lung tissues (n = 6 for each group) from different groups were weighed, homogenized, and centrifuged at 10,000 rpm for 10 min at 4 °C to separate the supernatants. According to manufacturer's instructions, the protein concentrations of interleukin-6 (IL-6), interleukin-1 beta (IL-1β), and tumor necrosis factor-alpha (TNF-α) in serum and the protein contents of toll-like receptor 4 (TLR4), nuclear factor-kappa B (NF-κB), IL-6, IL-1β, and TNF-α in lung samples were detected using the ELISA method.

Molecular Docking

The chemical structures of the identified compounds were obtained from PubChem database (https://pubchem.ncbi.nlm.nih.gov/) followed by format conversion with OpenBabel (Version 2.3.2) software. The X-ray crystal structures of target proteins were searched from the Protein Data Bank (PDB) database (http://www.rcsb.org/pdb/) and the PDB format files of TLR4 (PDB: 3FXI) and NF-κB p65 (PDB: 1NFI) were downloaded. Subsequently, we employed the AutoDock (Version 4.2.6) software to execute the operations of dehydration and hydrogenation, and then the files of protein receptors and compound ligands were exported in PDBQT format. The AutoDock Vina (Version 1.2.0) software was applied for docking simulation, and the optimal pose was selected to analyze the interaction between receptors and ligands. The visualization of docking results was performed using the PyMOL (Version 2.5) software. The binding energy ≤−5.0 kcal/mol was considered as acceptable docking affinity.[38] A smaller value indicated better binding activity.

Statistical Analysis

All the experimental data were presented as mean ± SD, and SPSS (Version 16.0) software (SPSS, Inc., Chicago, IL, United States) was employed for statistical analysis. The comparison between two groups was carried out using the Student's two-tailed t-test and comparisons among multiple groups were performed using the one-way analysis of variance (ANOVA) followed by Dunnett's t-test. The statistical significance was defined as $P < 0.05$ and GraphPad Prism (Version 8.0.2) software (GraphPad Software, Inc., La Jolla, CA, United States) was used for graphing.

Results

QFHXD Intervention Mitigated ALI and Systemic Inflammation Stimulated by LPS

To evaluate the anti-ALI effect of QFHXD, the experimental mice experienced LPS modeling after 8 times of intragastric administration of QFHXD (Figure 1A). After 24 h of LPS stimulation, the histopathological changes in each group were observed using H&E staining. In contrast to the normal tissue morphology of control mice without LPS treatment, the obvious lesions, including alveolar dilatation, thickening of alveolar walls, pulmonary edema, and massive inflammatory cell accumulation, were observed in the lung tissues of the model group (Figure 1B). Fortunately, different doses of QFHXD pretreatment effectively ameliorated the serious histopathological damages induced by intratracheal administration of LPS (Figure 1B). In addition, the results of ELISA detection showed that the concentrations of IL-6, IL-1β, and TNF-α in serum were significantly upregulated in the model group due to systematic inflammation induced by LPS stimulation (Figure 1C–E). However, intervention with QFHXD at a high dose could markedly downregulate these pro-inflammatory levels of serum
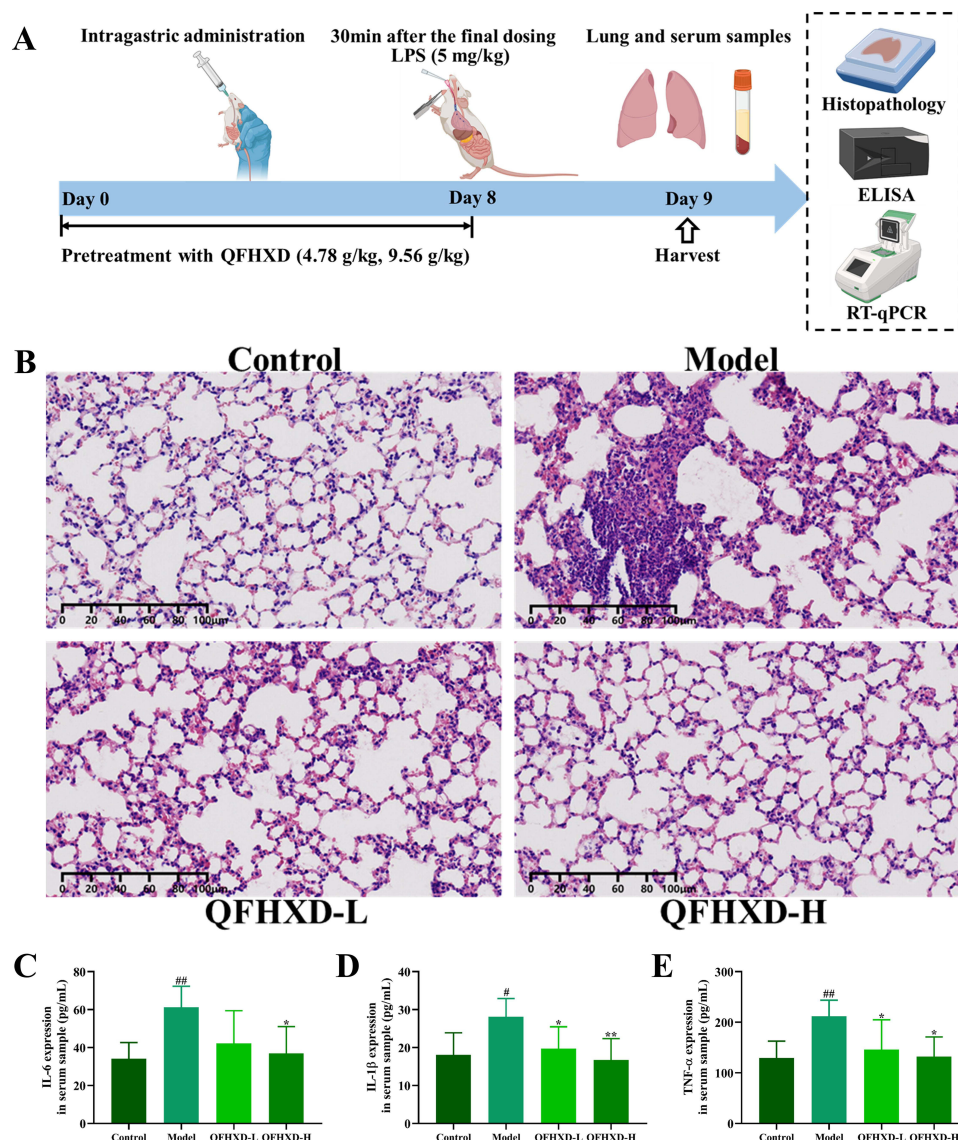
Figure 1 Pretreatment with QFHXD prevented lung lesions and inflammation caused by LPS administration. (**A**) The schematic diagram of experimental design. (**B**) The representative images of efficacy evaluation of QFHXD pretreatment against pathological damages (×200 magnification, scale bar: 100 μm, n = 4). Pretreatment with different doses of QFHXD could relieve the histopathological alterations in ALI mice. The detection of IL-6 (**C**), IL-1β (**D**), and TNF-α (**E**) contents in serum samples of each group (n = 6). Compared with the model group, high dosage of QFHXD administration clearly decreased the levels of pro-inflammatory cytokines. Data are presented as the mean ± SD. [#]$P < 0.05$, and [##]$P < 0.01$ versus the control group; *$P < 0.05$, and **$P < 0.01$ versus the model group. Model, LPS; QFHXD-L, QFHXD low dose (4.78 g/kg); QFHXD-H, QFHXD high dose (9.56 g/kg).

samples (Figure 1C–E). These data suggested that QFHXD pretreatment effectively reduced LPS-induced histopathological changes and systemic inflammation.

Chemical Characterization of Main Compositions in QFHXD

To clarify chemical components of QFHXD, the base peak chromatograms of QFHXD in both negative and positive ion modes were captured using UPLC-Q-TOF-MS/MS (Figure 2A and B). After data matching of literatures and public databases, a total of 99 compounds were tentatively characterized as listed in Supplementary Table S2. Among them, 18 ingredients in QFHXD sample, including adenosine, gallic acid, danshensu, loganic acid, (+)-catechin, chlorogenic acid, amygdalin, epicatechin, paeoniflorin, rutin, luteoloside, narirutin, hesperidin, rosmarinic acid, salvianolic acid B, baicalin, salvianolic acid A, and oroxylin A-7-O-glucuronide, were further identified via comparing the main MS/MS fragments and retention times with those of standard substances. In addition, the MS/MS-based molecular network was constructed using GNPS to
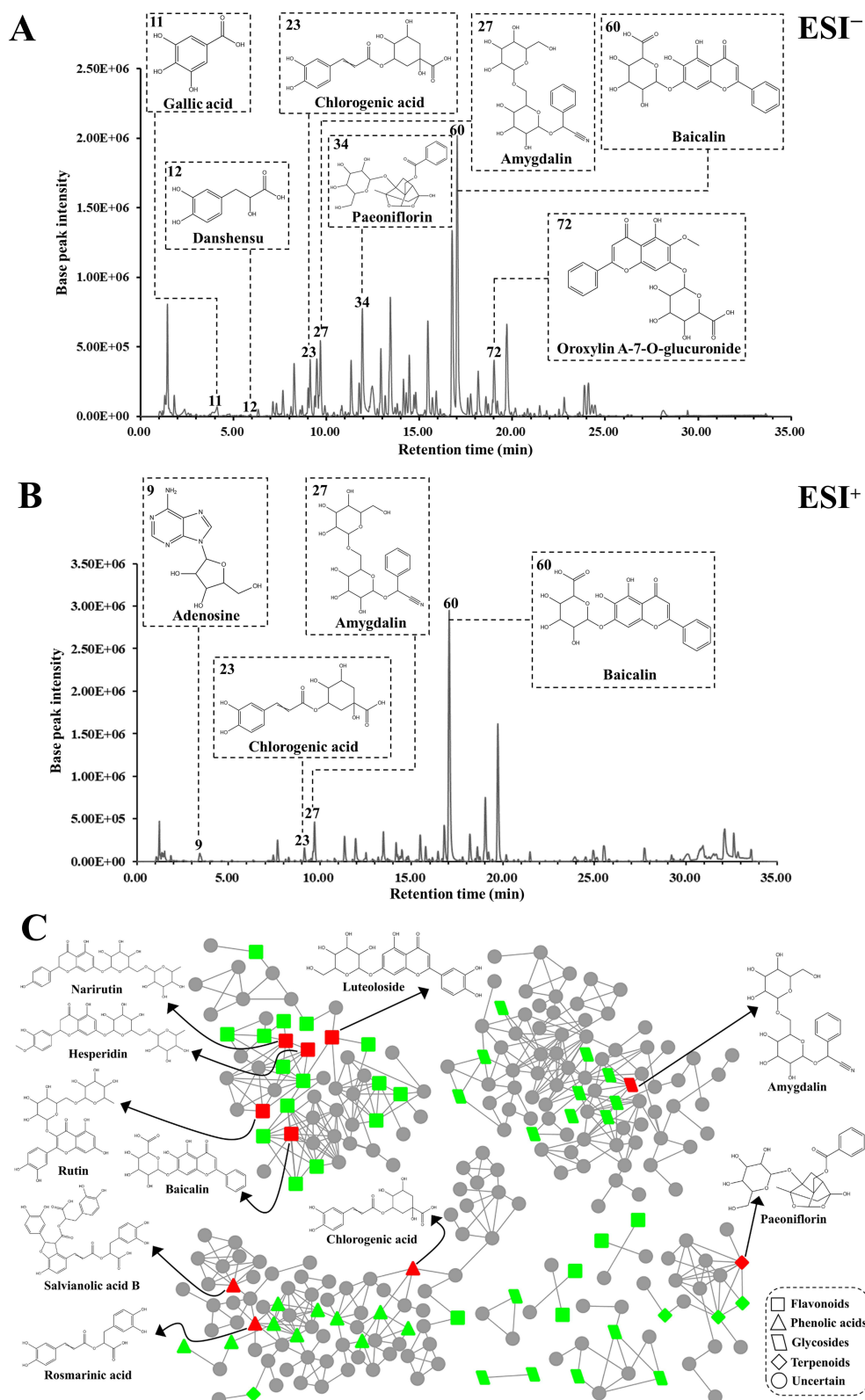
Figure 2 Chemical profiling of main components in QFHXD. The base peak chromatograms and representative chemical structures of QFHXD sample in both negative ion mode (**A**) and positive ion mode (**B**). (**C**) Molecular networking of major compounds in QFHXD. Red color represents compounds identified by comparison with standards. Green color represents compounds deduced by GNPS library. Gray color represents uncertain compounds. Different shapes represent different types of compounds.

assist in the cluster and identification of main compounds in QFHXD. Each recognized component from the raw data was displayed as a node with corresponding shape, and the similarity between the nodes was represented as the link. As shown in Figure 2C, flavonoids, glycosides, phenolic acids, and terpenoids constituted the main clusters in molecular network, which were consistent with the results of above identification (Supplementary Table S2). Especially, 10 identified compounds, including chlorogenic acid, amygdalin, paeoniflorin, rutin, luteoloside, narirutin, hesperidin, rosmarinic acid, salvianolic acid B, and baicalin, were confirmed again by MSMN.

Decoding the Possible Molecular Mechanisms of QFHXD Against ALI

To elucidate the underlying mechanisms of QFHXD intervention in rescuing ALI, we conducted a network pharmacology study. Through the retrieval of multiple online databases, 901 ALI-related genes were acquired (Figure 3A). To construct the component-target network, 18 definitely identified ingredients were designated (Supplementary Table S2), and 340 associated targets were collected. The top correlation between main compounds and targets was displayed in Figure 3B. A total of 153 overlapped targets (Supplementary Table S3) were determined by overlapping two datasets of
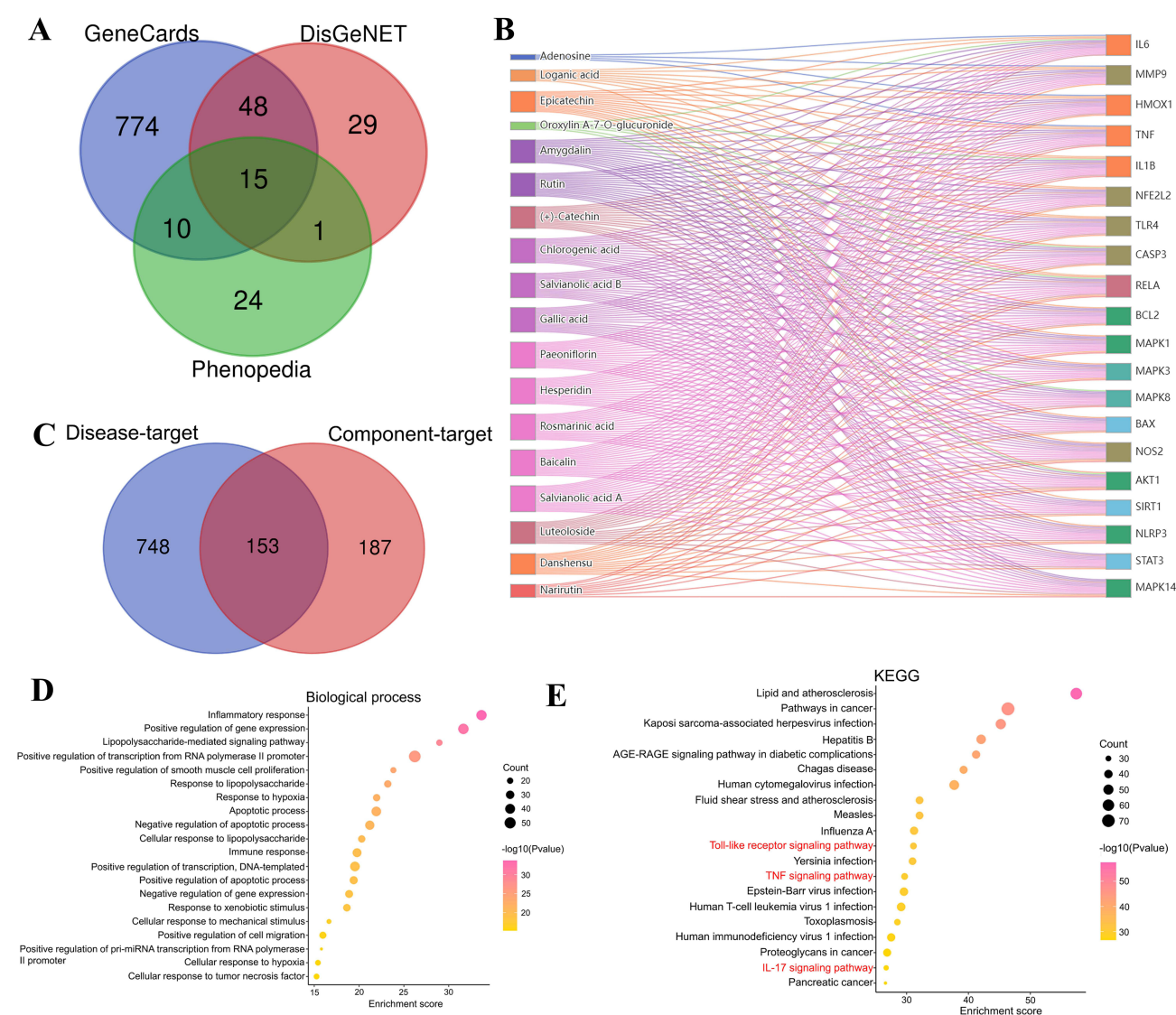

Figure 3 Construction of ingredient-target-disease network and the enrichment analyses of GO and KEGG. (**A**) Venn diagram of ALI related targets. (**B**) The main component-top target network. (**C**) Venn diagram of two data sets. A total of 153 overlapped targets were identified as potential targets for QFHXD intervention against ALI. (**D**) GO enrichment analysis. According to the enrichment score and enriched gene numbers, inflammatory response ranked the top of GO terms. (**E**) KEGG pathway enrichment analysis. Top 20 significantly enriched signaling pathways were displayed according to the ranking criteria. Inflammation related pathways were highlighted in red.

disease-target and component-target networks (Figure 3C). The list of compound-target-disease network was uploaded to DAVID for follow-up analysis. Among the top 20 significantly sorted GO terms, inflammatory response, ranked the first with the highest enrichment score and relatively more involved genes, could be considered as the key biological process accounting for anti-ALI action of QFHXD (Figure 3D). Coincidentally, the inflammation related pathways, including toll-like receptor signaling pathway, TNF signaling pathway, and IL-17 signaling pathway, were observably enriched (Figure 3E). The analytical results indicated that inflammatory mechanisms were strongly associated with the lung protection and anti-inflammatory activities of QFHXD in response to LPS stimulation.

Determination of Core Genes Participated in the Inflammatory Regulation of QFHXD Against ALI

To further pinpoint the core genes regulated by QFHXD in response to ALI, we performed the detailed analyses of 153 overlapped targets. After establishing a PPI network of overlapped genes (Supplementary Figure S1), the tightest linked cluster (90 nodes and 3339 edges) was captured with MCODE score of 75.034 (Figure 4A). We then utilized the cytoHubba module of Cytoscape to screen the top nodes of the cluster based on Degree and DMNC methods. According to the results of different methods, top 20 nodes were, respectively, visualized (Figure 4B and C), and the detailed information was listed in Supplementary Tables S4 and S5. Considering the importance of inflammatory mechanisms in therapeutic effect of QFHXD and the progression of ALI, we united inflammatory response-related genes, top nodes obtained by cytoHubba module, and toll-like receptor signaling pathway-related targets to recognize the hub targets involved in the inflammatory regulation of QFHXD in response to ALI. As shown in Figure 4D and E, 10 key genes, including TLR4, MYD88, RELA, NFKB1, IL6, IL1B, TNF, CXCL8, FOS, and AKT1, were determined as candidate core targets for deciphering the lung protection and anti-inflammation effects of QFHXD against ALI, which deserved follow-up experimental verification.

QFHXD Pretreatment Inhibited ALI by Regulating TLR4/NF-κB Pathway Mediated Inflammation

Combined with the main component-top target network (Figure 3B) and selected candidate hub targets (Figure 4D and E), five candidate hub genes, including TLR4, RELA, IL6, IL1B, and TNF, were chosen to shed light on the inflammatory regulation of QFHXD against ALI. Hence, RT-qPCR and ELISA experiments were performed to assess the mRNA and protein levels of lung tissues from each group. Consistent with the previous results of histopathological observation and serum detection, LPS stimulation resulted in an obvious inflammatory reaction in lung tissues. Abnormally increased mRNA and protein levels of pro-inflammatory mediators, including TLR4, NF-κB, IL-6, IL-1β, and TNF-α, were detected in impaired lung samples compared to those in the control group (Figure 5A–J). In contrast, successive pretreatment with QFHXD exerted significant anti-inflammatory action. On the one hand, the transcriptional levels of pro-inflammatory factors in damaged lung tissues were observably lowered after different doses of QFHXD intervention compared to ALI mice without drug pretreatment (Figure 5A–E). On the other hand, pretreatment with high dose of QFHXD obviously reversed the abnormally elevated protein concentrations of above pro-inflammatory mediators in lung samples of ALI mice (Figure 5F–J). These data suggested that the regulatory role in TLR4/NF-κB pathway mediated inflammation partly contributed to the beneficial effect of QFHXD against ALI.

Identification of Potential Active Ingredients in QFHXD Against ALI

Based on the close relationship between anti-ALI action of QFHXD and TLR4/NF-κB pathway mediated inflammation, molecular docking was performed to identify the potential anti-ALI active substances. In this work, the representative components, including gallic acid, danshensu, loganic acid, chlorogenic acid, amygdalin, paeoniflorin, rutin, luteoloside, narirutin, hesperidin, rosmarinic acid, salvianolic acid B, baicalin, salvianolic acid A, and oroxylin A-7-O-glucuronide were designated as ligands, while the key targets, including TLR4 and NF-κB p65, were selected as receptors. Subsequently, the interactional pattern between ligands and receptors was investigated. The docking results showed that the docking scores of ligands and receptor proteins were all less than −5 kcal/mol, indicating the good affinity of these components with core target
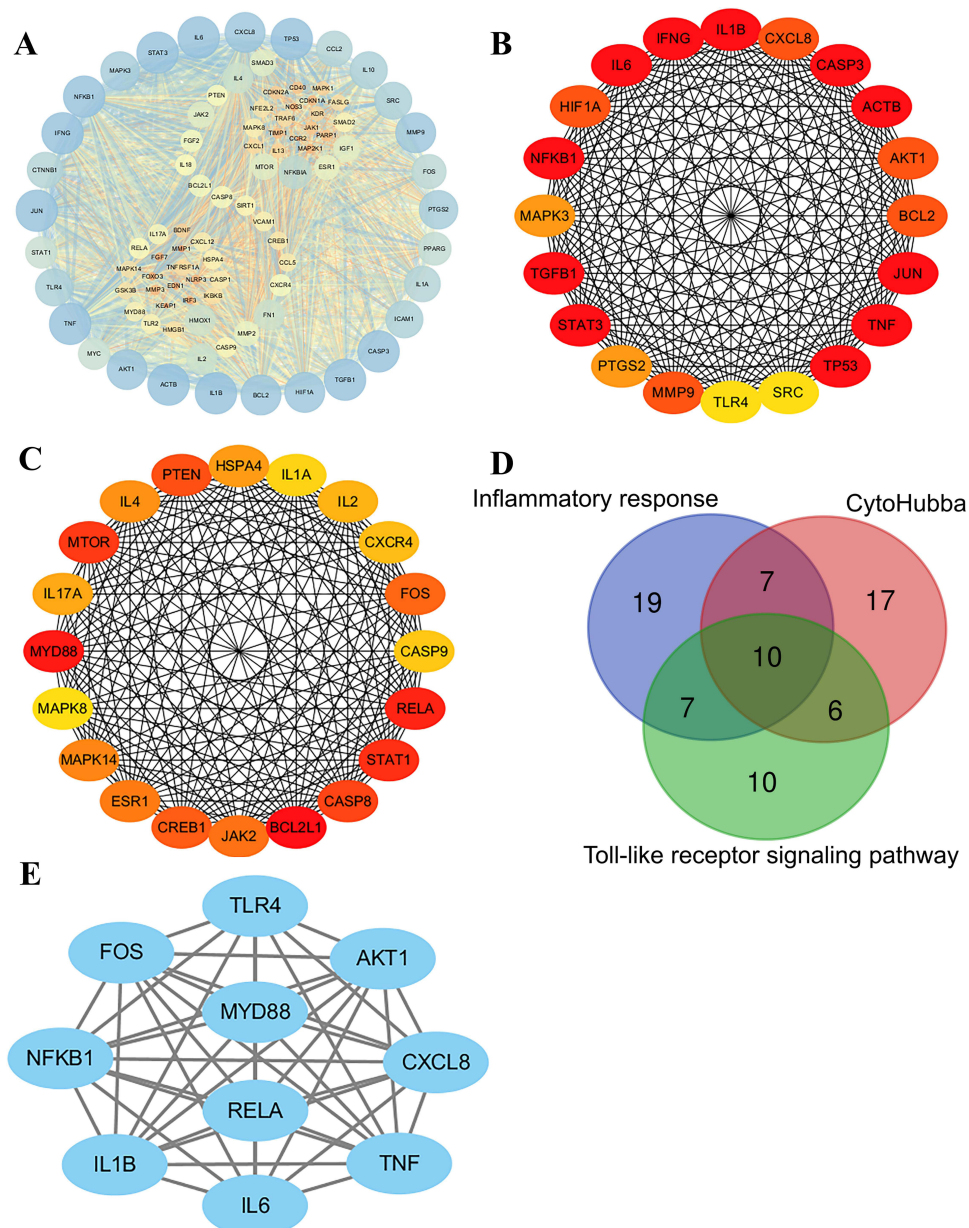
Figure 4 The PPI network analysis and identification of key targets involved in anti-ALI mechanisms of QFHXD. (**A**) The PPI network of MCODE module analysis. The most significant cluster with 90 nodes and 3339 edges was extracted. The larger size of a node represented a higher value of degree. (**B**) cytoHubba module analysis based on Degree method. CASP3, JUN, ACTB, IL6, TGFB1, TNF, NFKB1, IFNG, IL1B, STAT3 et al, were the top nodes ranked by Degree method. The deeper color represented the more importance in the PPI network. (**C**) cytoHubba module analysis based on DMNC method. BCL2L1, MYD88, RELA, STAT1, MTOR, CASP8, PTEN, CREB1, FOS, JAK2 et al, were the top nodes ranked by DMNC method. The deeper color represented the more importance in the PPI network. (**D**) Venn diagram for the confirmation of candidate core targets. Through integrating inflammatory response related genes, top nodes acquired by cytoHubba module analysis, and toll-like receptor signaling pathway related genes, 10 hub targets were finally confirmed. (**E**) The PPI network of 10 candidate hub targets.

proteins (Figure 6A–L and Supplementary Figure S2). Among them, the top docking scores between main compounds and target protein TLR4 were −8.0 kcal/mol for hesperidin and −7.7 kcal/mol for narirutin, luteoloside, and salvianolic acid A (Figure 6A–D). Meanwhile, the top docking scores between main compounds and target protein NF-κB p65 were −8.5 kcal/mol for narirutin and −8.2 kcal/mol for hesperidin (Figure 6G and H). The above results revealed the anti-ALI potential of these main components targeting to TLR4/NF-κB mediated inflammation.
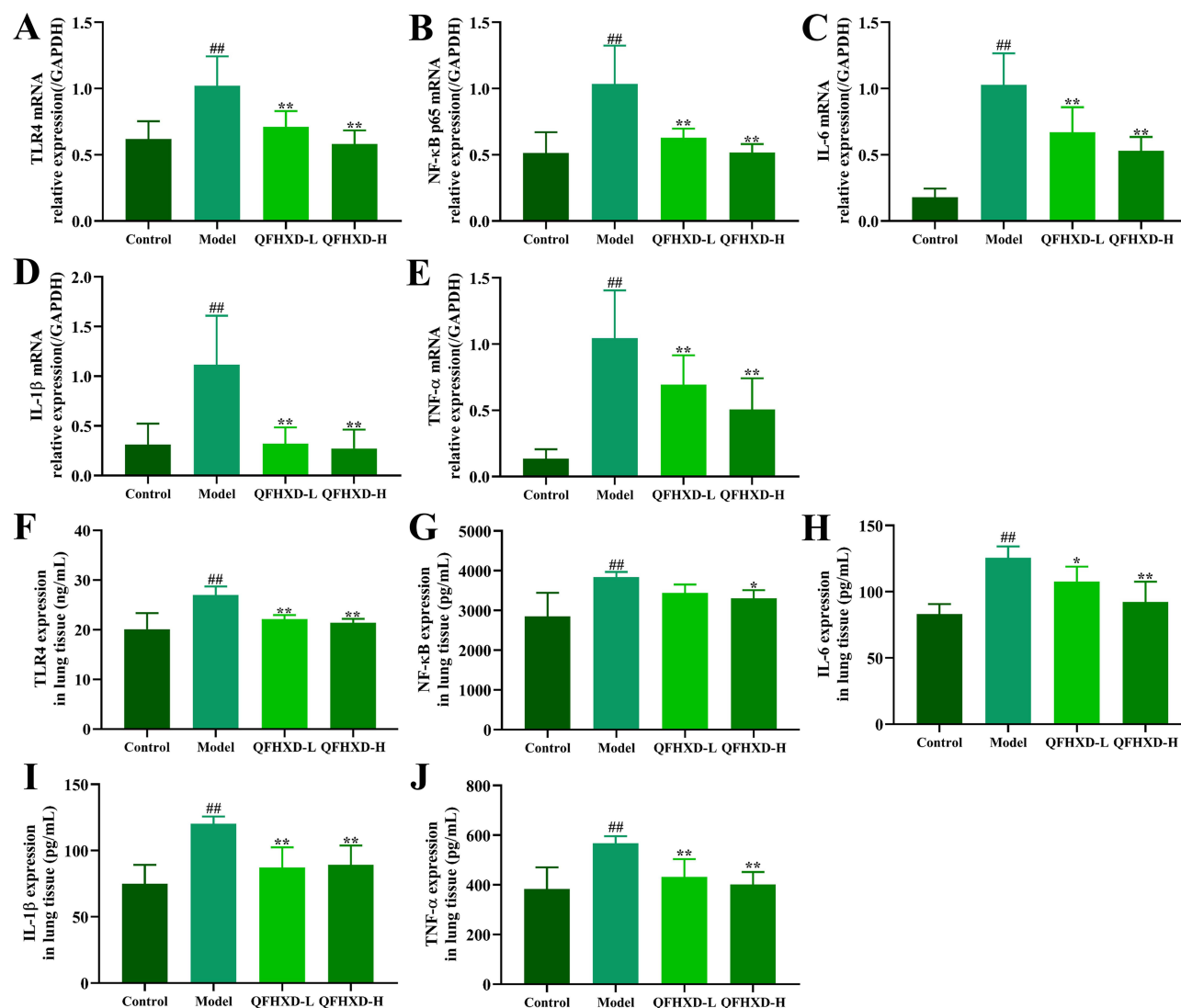
Figure 5 Experimental verification of the potential targets related to anti-ALI action of QFHXD. Relative expression levels of TLR4 (**A**), NF-κB p65 (**B**), IL-6 (**C**), IL-1β (**D**), and TNF-α (**E**) mRNA were measured by RT-qPCR (n = 5). Results were normalized to GAPDH. The detection of TLR4 (**F**), NF-κB (**G**), IL-6 (**H**), IL-1β (**I**), and TNF-α (**J**) protein concentrations in lung samples of each group (n = 6). Compared with the model group, high dose of QFHXD pretreatment significantly decreased the mRNA and protein levels of pro-inflammatory factors in damaged lung tissues of ALI mice. Data are presented as the mean ± SD. $^{\#\#}P < 0.01$ versus the control group; $^{*}P < 0.05$, and $^{**}P < 0.01$ versus the model group. Model, LPS; QFHXD-L, QFHXD low dose (4.78 g/kg); QFHXD-H, QFHXD high dose (9.56 g/kg).

Narirutin Pretreatment Played Anti-ALI Role by Modulating TLR4/NF-κB Mediated Inflammation

Animal and molecular experiments were performed to verify the accuracy of molecular docking. Based on the top docking scores and literature retrieval, the anti-ALI effect of narirutin and its underlying mechanism of inflammatory regulation were investigated (Figure 7A). In contrast to the detrimental histopathological changes (thickening of alveolar walls, edema and inflammatory cell infiltration) caused by LPS stimulation, pretreatment with different doses of narirutin effectively reduced pathological damage to lung tissues (Figure 7B). Subsequently, we monitored the protein expression of inflammatory mediators in lung tissues of each group using the ELISA kits. As expected, intervention with different doses of narirutin significantly decreased the abnormally increased protein contents of TLR4, NF-κB, IL-6, and TNF-α in lung samples of ALI mice (Figure 7C–F). In addition, the upregulated protein levels of IL-1β in impaired lung tissues of model group were markedly downregulated after high dose of narirutin pretreatment (Figure 7G). These data suggested that narirutin could be considered as an active substance against ALI via regulating TLR4/NF-κB mediated inflammation.
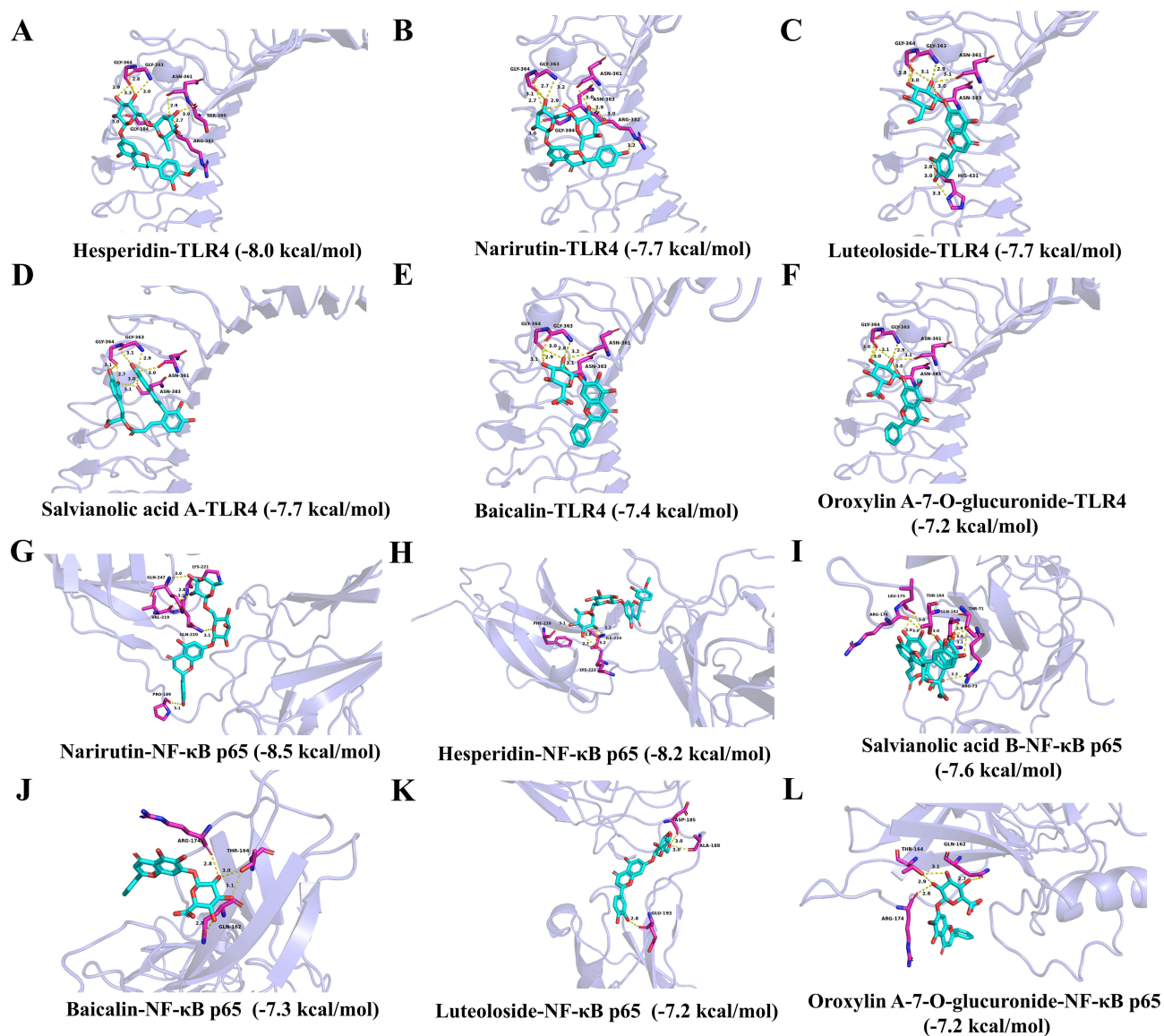
Figure 6 Identification of potential anti-ALI constituents via performing molecular docking. Molecular models of hesperidin (**A**), narirutin (**B**), luteoloside (**C**), salvianolic acid A (**D**), baicalin (**E**), and oroxylin A-7-O-glucuronide (**F**) binding to hub protein TLR4. Molecular models of narirutin (**G**), hesperidin (**H**), salvianolic acid B (**I**), baicalin (**J**), luteoloside (**K**), and oroxylin A-7-O-glucuronide (**L**) binding to hub protein NF-κB p65.

Discussion

ALI and ARDS are the life-threatening clinical syndromes with stubbornly high morbidity and mortality, resulting in increased healthcare burden.[39] In particular, COVID-19 pandemic has further exacerbated the seriousness and urgency of the problem.[40] Currently, clinical treatments for ALI/ARDS commonly include supportive therapy and pharmacological intervention.[4] However, the limitations, such as ventilator-induced lung injury and adverse side effects of Western drugs, lead to a persistent lack of safe and effective therapies in clinical practice.[5,6,41] Owing to the complexity of the pathogenesis involved in ALI/ARDS, patient-specific therapies and combination therapies targeting to multiple targets/ pathways are recommended.[42] In China, TCM prescriptions with multi-component and multi-target/pathway features provide a reliable option for pharmacotherapy of ALI/ARDS. For instance, Xuanfei Baidu formula, Huashi Baidu formula, Lianhua Qingwen formula, and Jinhua Qinggan formula have been proven to have a definite efficacy against COVID-19 and ALI.[43–46] In addition, the active ingredients of CMs have become a valuable source for discovering and developing novel anti-ALI drugs.[47,48]
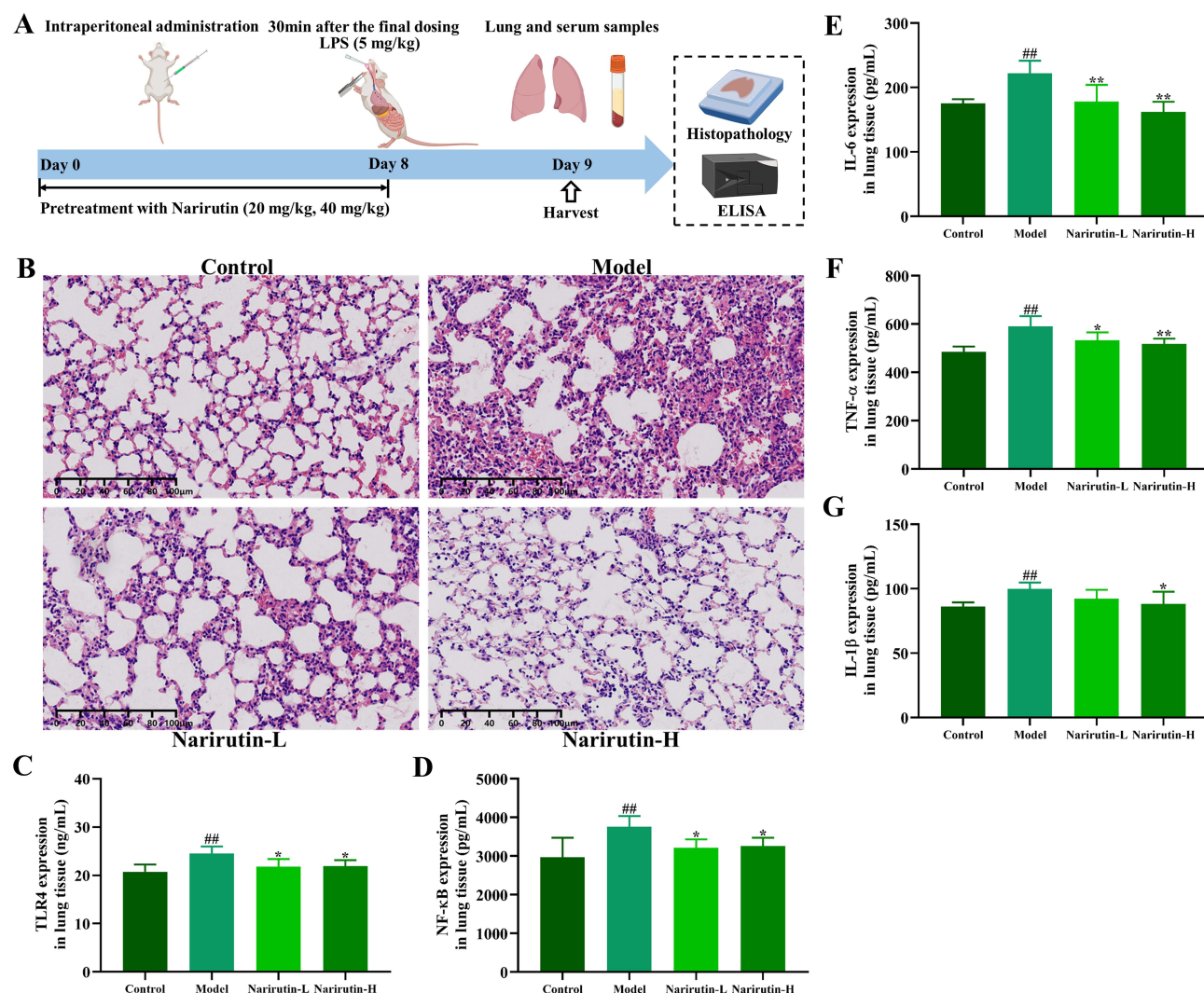
Figure 7 Narirutin pretreatment prevented LPS-induced ALI via inflammatory regulation. (**A**) The schematic diagram of experimental design. (**B**) The representative images of histopathological observation of narirutin pretreatment against ALI (×200 magnification, scale bar: 100 μm, n = 4). Pretreatment with different doses of narirutin could mitigate lung lesions caused by LPS stimulation. The measurement of TLR4 (**C**), NF-κB (**D**), IL-6 (**E**), TNF-α (**F**) and IL-1β (**G**) protein levels in lung tissues (n = 6). Pretreatment with narirutin at a dose of 40 mg/kg notably downregulated the protein contents of pro-inflammatory factors in impaired lung tissues compared to those in ALI mice. Data are presented as the mean ± SD. $^{##}P < 0.01$ versus the control group; $*P < 0.05$, and $**P < 0.01$ versus the model group. Model, LPS; Narirutin-L, narirutin low dose (20 mg/kg); Narirutin-H, narirutin high dose (40 mg/kg).

QFHXD, which consists of 18 CMs, has remarkable efficacy as a hospital agreement prescription for the treatment of pulmonary diseases. However, the pharmacological action of QFHXD against ALI has yet to be reported, let alone questions of underlying functional mechanisms and anti-ALI active substances. Airway administration of LPS is an accepted method to construct a well-characterized and highly repeatable ALI animal model.[49] Indeed, after intratracheal LPS infusion, diffuse alveolar injury, thickening of alveolar walls, edema, and inflammatory cell infiltration were observed in damaged lung tissues by H&E staining (Figure 1B). In addition, significantly elevated levels of pro-inflammatory cytokines were found in serum, indicating the occurrence of uncontrollable inflammation after LPS stimulation (Figure 1C–E). Through comparing the histopathological changes and serum inflammatory concentrations among different groups, we first presented in vivo evidence of the beneficial effect of QFHXD against LPS-induced lung injury and inflammation (Figure 1).

To further decipher the possible mechanisms accounting for the anti-ALI effect of QFHXD, a compound-target-disease network was established based on 18 unambiguously identified main components of QFHXD (Figure 3 and Supplementary Table S2). Interestingly, inflammatory response and inflammation-related pathways were obviously enriched in accordance with the results of GO and KEGG enrichment analyses (Figure 3D and E), suggesting a close connection between

inflammatory regulation and anti-ALI action of QFHXD. Notably, several pharmacological studies have shown that the major CMs of QFHXD, including Jinyinhua, Pugongying, Lianqiao, Huangqin, Jiegeng, Danshen, Chaihu, and Chenpi, could alleviate LPS-induced ALI via modulating inflammatory mechanisms.[15–19,22,23,50] These reports further supported the deduction of inflammatory regulation of QFHXD against ALI.

The dysregulated inflammatory response is a major pathogenic mechanism of ALI/ARDS.[51] The inflammatory cascade of triggering ALI involves various intercellular interaction (eg, neutrophils, macrophages, endothelial cells, and lymphocytes) and the release of pro-inflammatory mediators.[52] The increasing studies believed that the TLR4/NF-κB pathway played an important role in rapidly launching intracellular inflammatory pathways in response to LPS challenge.[53–55] As one of the best-characterized pattern recognition receptors, TLR4 is known to specifically recognize LPS. The binding of LPS and TLR4 leads to the activation of NF-κB through initiating a signaling cascade.[56] Once activated, NF-κB p65 rapidly translocates to the nucleus and triggers the transcription of specific target genes such as IL-6, IL-1β, and TNF-α.[57,58] As typical pro-inflammatory cytokines, the markedly elevated levels of IL-6, IL-1β, and TNF-α were found in blood samples and bronchoalveolar lavage fluid of ALI patients, which predicted poor clinical outcomes.[59] Coincidentally, 5 candidate hub targets, including TLR4, RELA, IL6, IL1B, and TNF, were finally selected to uncover the functional mechanisms of QFHXD against ALI according to the results of network analyses (Figures 3B and 4). The subsequent experimental verification showed that QFHXD pretreatment effectively reduced the abnormally increased mRNA and protein levels of TLR4, NF-κB, IL-6, IL-1β, and TNF-α in damaged lung tissues of ALI mice (Figure 5). The current data presented the fact that the QFHXD intervention obviously suppressed the TLR4/NF-κB pathway mediated inflammatory reaction, thereby ameliorating ALI in mice.

Molecular docking has been of great value in the discovery of novel promising compounds.[60] To identify the potential anti-ALI active ingredients targeting to TLR4/NF-κB pathway, molecular docking was carried out to predict the binding strength and affinity of the ligands (main compounds of QFHXD) and receptors (TLR4 and NF-κB p65) according to the preferred orientation of compound relative to receptor. The docking results revealed a good affinity of these components with target proteins (Figure 6A–L and Supplementary Figure S2). Previous studies have reported that hesperidin, baicalin, and danshensu could inhibit TLR4/NF-κB pathway mediated inflammation to exert anti-ALI activity.[61–63] The main compounds, such as amygdalin, rutin, salvianolic acid B, paeoniflorin, rosmarinic acid, salvianolic acid A, chlorogenic acid, and rutin, and were also found to mitigate ALI via inflammatory mechanisms.[64–71] These reports verified the reliability of docking results. In addition, considering the top docking scores and the unavailability of literature, we further investigated the anti-ALI action of narirutin and its anti-inflammatory mechanism. Narirutin pretreatment was observed to reduce LPS-induced lung lesions and lower the protein contents of pro-inflammatory factors in lung tissues of ALI mice (Figure 7). Here, we first provided strong evidence of narirutin as one of active substances in QFHXD against anti-ALI via reducing TLR4/NF-κB mediated inflammation.

Overall, the current research demonstrated the anti-ALI effect of QFHXD and the underlying molecular mechanisms and active compounds, and some limitations still exist. For instance, the beneficial effects of QFHXD against ALI require further evaluation in clinical research. In follow-up studies, more molecular biology experiments should be performed to confirm the regulatory effects of QFHXD and its active component narirutin on TLR4/NF-κB mediated inflammation. Other potential anti-ALI ingredients of QFHXD (eg, hesperidin and luteoloside) need to be further defined via performing additional in vivo and in vitro experiments. Overcoming these limitations will contribute to the development of novel anti-ALI drugs and the expansion of clinical application of QFHXD in the treatment of lung diseases.

Conclusion

In summary, the present work provides the first evidence for the protective effects of QFHXD and its active constituent narirutin against LPS-induced ALI, which may be partly attributed to the regulation of TLR4/NF-κB mediated inflammatory reaction. These interesting findings may provide a novel therapeutic option for ALI patients.

Abbreviations

ALI, acute lung injury; ANOVA, one-way analysis of variance; ARDS, acute respiratory distress syndrome; CE, collision energy; CMs, Chinese medicines; COVID-19, Coronavirus Disease 2019; CUR, curation gas; DAVID, Database for

Annotation, Visualization and Integration Discovery; DMNC, density of maximum neighborhood component; DMSO, dimethyl sulfoxide; DP, declustering potential; ELISA, enzyme-linked immunosorbent assay; ESI$^+$, positive electrospray ionization; ESI$^-$, negative electrospray ionization; GAPDH, glyceraldehyde 3-phosphate dehydrogenase; GNPS, Global Natural Products Social Molecular Networking; GO, Gene Ontology; H&E, Hematoxylin & Eosin; HERB, high-throughput experiment- and reference-guided database of traditional Chinese medicine; IDA, information-dependent acquisition; IL-1β, Interleukin-1 beta; IL-6, Interleukin-6; KEGG, Kyoto Encyclopedia of Genes and Genomes; LPS, lipopolysaccharide; MCODE, Molecular Complex Detection; MSMN, mass spectrometry molecular networking; NETs, neutrophil extracellular traps; NF-κB, nuclear factor-kappa B; PDB, Protein Data Bank; PPI, protein–protein interaction; QFHXD, Qingfei Huoxue decoction; RT-qPCR, real-time quantitative polymerase chain reaction; STRING, Search Tool for Recurring Instances of Neighboring Genes; TCM, traditional Chinese medicine; TCMSP, Traditional Chinese Medicine Systems Pharmacology Database and Analysis Platform; TLR4, toll-like receptor 4; TNF-α, tumor necrosis factor-alpha.

Acknowledgments

Funding

Disclosure
The authors declare that there are no conflicts of interest associated with this manuscript and no significant financial support for this work that would influence its outcome.

References

1. Long ME, Mallampalli RK, Horowitz JC. Pathogenesis of pneumonia and acute lung injury. *Clin Sci*. 2022;136(10):747–769. doi:10.1042/CS20210879
2. Narota A, Puri G, Singh VP, Kumar A, Naura AS. COVID-19 and ARDS: update on preventive and therapeutic venues. *Curr Mol Med*. 2022;22(4):312–324. doi:10.2174/1566524021666210408103921
3. Bos LDJ, Ware LB. Acute respiratory distress syndrome: causes, pathophysiology, and phenotypes. *Lancet*. 2022;400(10358):1145–1156. doi:10.1016/S0140-6736(22)01485-4
4. Mokra D. Acute lung injury-from pathophysiology to treatment. *Physiol Res*. 2020;69(Suppl 3):S353–S366. doi:10.33549/physiolres.934602
5. Mokra D, Mikolka P, Kosutova P, Mokry J. Corticosteroids in acute lung injury: the dilemma continues. *Int J Mol Sci*. 2019;20(19):4765. doi:10.3390/ijms20194765
6. Mokra D, Mokry J. Phosphodiesterase inhibitors in acute lung injury: what are the perspectives. *Int J Mol Sci*. 2021;22(4):1929. doi:10.3390/ijms22041929
7. Ding Z, Zhong R, Xia T, et al. Advances in research into the mechanisms of Chinese Materia Medica against acute lung injury. *Biomed Pharmacother*. 2020;122:109706. doi:10.1016/j.biopha.2019.109706
8. Ma XL, Chen YR, Shen FY, Yu SQ, Zhu ZH, Zhao HJ. Research progress on therapeutic effect and mechanism of traditional Chinese medicine in acute lung injury. *Chin J Mod Appl Pharm*. 2022;39(2):269–276. Chinese. doi:10.13748/j.cnki.issn1007-7693.2022.02.022
9. Wang J, Wu Q, Ding L, et al. Therapeutic effects and molecular mechanisms of bioactive compounds against respiratory diseases: traditional Chinese medicine theory and high-frequency use. *Front Pharmacol*. 2021;12:734450. doi:10.3389/fphar.2021.734450
10. Mokra D, Kosutova P. Biomarkers in acute lung injury. *Respir Physiol Neurobiol*. 2015;209:52–58. doi:10.1016/j.resp.2014.10.006
11. Lesur I, Textoris J, Loriod B, et al. Gene expression profiles characterize inflammation stages in the acute lung injury in mice. *PLoS One*. 2010;5(7):e11485. doi:10.1371/journal.pone.0011485
12. Grommes J, Soehnlein O. Contribution of neutrophils to acute lung injury. *Mol Med*. 2011;17(3–4):293–307. doi:10.2119/molmed.2010.00138
13. Song C, Li H, Li Y, et al. NETs promote ALI/ARDS inflammation by regulating alveolar macrophage polarization. *Exp Cell Res*. 2019;382(2):111486. doi:10.1016/j.yexcr.2019.06.031
14. Fadanni GP, Calixto JB. Recent progress and prospects for anti-cytokine therapy in preclinical and clinical acute lung injury. *Cytokine Growth Factor Rev*. 2023;71-72:13–25. doi:10.1016/j.cytogfr.2023.07.002

15. Liu C, Yin Z, Feng T, Zhang M, Zhou Z, Zhou Y. An integrated network pharmacology and RNA-Seq approach for exploring the preventive effect of Lonicerae japonicae flos on LPS-induced acute lung injury. *J Ethnopharmacol*. 2021;264:113364. doi:10.1016/j.jep.2020.113364

16. Ma C, Zhu L, Wang J, et al. Anti-inflammatory effects of water extract of Taraxacum mongolium hand.-Mazz on lipopolysaccharide-induced inflammation in acute lung injury by suppressing PI3K/Akt/mTOR signaling pathway. *J Ethnopharmacol*. 2015;168:349–355. doi:10.1016/j. jep.2015.03.068

17. Wang J, Luo L, Zhao X, et al. Forsythiae Fructuse extracts alleviates LPS-induced acute lung injury in mice by regulating PPAR-γ/RXR-α in lungs and colons. *J Ethnopharmacol*. 2022;293:115322. doi:10.1016/j.jep.2022.115322

18. Chen JJ, Huang CC, Chang HY, et al. Scutellaria baicalensis ameliorates acute lung injury by suppressing inflammation in vitro and in vivo. *Am J Chin Med*. 2017;45(1):137–157. doi:10.1142/S0192415X17500100

19. Zhou Y, Jin T, Gao M, et al. Aqueous extract of Platycodon grandiflorus attenuates lipopolysaccharide-induced apoptosis and inflammatory cell infiltration in mouse lungs by inhibiting PI3K/Akt signaling. *Chin Med*. 2023;18(1):36. doi:10.1186/s13020-023-00721-z

20. Liu C, Zhen D, Du H, et al. Synergistic anti-inflammatory effects of peimine, peiminine, and forsythoside a combination on LPS-induced acute lung injury by inhibition of the IL-17-NF-κB/MAPK pathway activation. *J Ethnopharmacol*. 2022;295:115343. doi:10.1016/j.jep.2022.115343

21. Liu X, Jin X, Yu D, Liu G. Suppression of NLRP3 and NF-κB signaling pathways by α-Cyperone via activating SIRT1 contributes to attenuation of LPS-induced acute lung injury in mice. *Int Immunopharmacol*. 2019;76:105886. doi:10.1016/j.intimp.2019.105886

22. Xie JY, Di HY, Li H, Cheng XQ, Zhang YY, Chen DF. Bupleurum chinense DC polysaccharides attenuates lipopolysaccharide-induced acute lung injury in mice. *Phytomedicine*. 2012;19(2):130–137. doi:10.1016/j.phymed.2011.08.057

23. Liu XX, Yu DD, Chen MJ, et al. Hesperidin ameliorates lipopolysaccharide-induced acute lung injury in mice by inhibiting HMGB1 release. *Int Immunopharmacol*. 2015;25(2):370–376. doi:10.1016/j.intimp.2015.02.022

24. Chen G, Ge D, Zhu B, Shi H, Ma Q. Salvia miltiorrhiza injection alleviates LPS-induced acute lung injury by adjusting the balance of MMPs/ TIMPs ratio. *Evid Based Complement Alternat Med*. 2020;2020:9617081. doi:10.1155/2020/9617081

25. Li G, Hu C, Liu Y, Lin H. Ligustilide, a novel SIRT1 agonist, alleviates lipopolysaccharide-induced acute lung injury through deacetylation of NICD. *Int Immunopharmacol*. 2023;121:110486. doi:10.1016/j.intimp.2023.110486

26. Li JH, Xu M, Xie XY, et al. Tanshinone IIA suppresses lung injury and apoptosis, and modulates protein kinase B and extracellular signal-regulated protein kinase pathways in rats challenged with seawater exposure. *Clin Exp Pharmacol Physiol*. 2011;38(4):269–277. doi:10.1111/j.1440-1681.2011.05498.x

27. Zhang X, Wang Y, Zhang K, et al. Discovery of tetrahydropalmatine and protopine regulate the expression of dopamine receptor D2 to alleviate migraine from Yuanhu Zhitong formula. *Phytomedicine*. 2021;91:153702. doi:10.1016/j.phymed.2021.153702

28. Li Z, Shi Y, Zhang X, et al. Screening immunoactive compounds of Ganoderma lucidum spores by mass spectrometry molecular networking combined with in vivo zebrafish assays. *Front Pharmacol*. 2020;11:287. doi:10.3389/fphar.2020.00287

29. Fang S, Dong L, Liu L, et al. HERB: a high-throughput experiment- and reference-guided database of traditional Chinese medicine. *Nucleic Acids Res*. 2021;49(D1):D1197–D1206. doi:10.1093/nar/gkaa1063

30. Ru J, Li P, Wang J, et al. TCMSP: a database of systems pharmacology for drug discovery from herbal medicines. *J Cheminform*. 2014;6:13. doi:10.1186/1758-2946-6-13

31. Stelzer G, Rosen N, Plaschkes I, et al. The GeneCards suite: from gene data mining to disease genome sequence analyses. *Curr Protoc Bioinformatics*. 2016;54:1.30.1–1.30.33. doi:10.1002/cpbi.5

32. Pinero J, Sauch J, Sanz F, Furlong LI. The DisGeNET cytoscape app: exploring and visualizing disease genomics data. *Comput Struct Biotechnol J*. 2021;19:2960–2967. doi:10.1016/j.csbj.2021.05.015

33. Yu W, Clyne M, Khoury MJ, Gwinn M. Phenopedia and Genopedia: disease-centered and gene-centered views of the evolving knowledge of human genetic associations. *Bioinformatics*. 2010;26(1):145–146. doi:10.1093/bioinformatics/btp618

34. Sherman BT, Hao M, Qiu J, et al. DAVID: a web server for functional enrichment analysis and functional annotation of gene lists (2021 update). *Nucleic Acids Res*. 2022;50(W1):W216–W221. doi:10.1093/nar/gkac194

35. Chen T, Liu YX, Huang LQ. ImageGP: an easy-to-use data visualization web server for scientific researchers. *iMeta*. 2022;1(1):e5. doi:10.1002/ imt2.5

36. Wang Y, Wu H, Han Z, et al. Guhong injection promotes post-stroke functional recovery via attenuating cortical inflammation and apoptosis in subacute stage of ischemic stroke. *Phytomedicine*. 2022;99:154034. doi:10.1016/j.phymed.2022.154034

37. Chin CH, Chen SH, Wu HH, Ho CW, Ko MT, Lin CY. cytoHubba: identifying hub objects and sub-networks from complex interactome. *BMC Syst Biol*. 2014;8(Suppl 4):S11. doi:10.1186/1752-0509-8-S4-S11

38. Guo X, Wu Y, Wang Q, et al. Huperzine A injection ameliorates motor and cognitive abnormalities via regulating multiple pathways in a murine model of Parkinson's disease. *Eur J Pharmacol*. 2023;956:175970. doi:10.1016/j.ejphar.2023.175970

39. Butt Y, Kurdowska A, Allen TC. Acute lung injury: a clinical and molecular review. *Arch Pathol Lab Med*. 2016;140(4):345–350. doi:10.5858/ arpa.2015-0519-RA

40. Swenson KE, Swenson ER. Pathophysiology of acute respiratory distress syndrome and COVID-19 lung injury. *Crit Care Clin*. 2021;37 (4):749–776. doi:10.1016/j.ccc.2021.05.003

41. Gattinoni L, Marini JJ, Collino F, et al. The future of mechanical ventilation: lessons from the present and the past. *Crit Care*. 2017;21(1):183. doi:10.1186/s13054-017-1750-x

42. Bosma KJ, Taneja R, Lewis JF. Pharmacotherapy for prevention and treatment of acute respiratory distress syndrome: current and experimental approaches. *Drugs*. 2010;70(10):1255–1282. doi:10.2165/10898570-000000000-00000

43. Li Z, Pan H, Yang J, et al. Xuanfei Baidu formula alleviates impaired mitochondrial dynamics and activated NLRP3 inflammasome by repressing NF-κB and MAPK pathways in LPS-induced ALI and inflammation models. *Phytomedicine*. 2023;108:154545. doi:10.1016/j.phymed.2022.154545

44. Wang Y, Jin X, Fan Q, et al. Deciphering the active compounds and mechanisms of HSBDF for treating ALI via integrating chemical bioinformatics analysis. *Front Pharmacol*. 2022;13:879268. doi:10.3389/fphar.2022.879268

45. Li S, Feng T, Zhang Y, et al. Lianhua Qingwen protects LPS-induced acute lung injury by promoting M2 macrophage infiltration. *J Ethnopharmacol*. 2024;320:117467. doi:10.1016/j.jep.2023.117467

46. Zhu Y, Han Q, Wang L, et al. Jinhua Qinggan granules attenuates acute lung injury by promotion of neutrophil apoptosis and inhibition of TLR4/ MyD88/NF-κB pathway. *J Ethnopharmacol*. 2023;301:115763. doi:10.1016/j.jep.2022.115763

47. He YQ, Zhou CC, Yu LY, et al. Natural product derived phytochemicals in managing acute lung injury by multiple mechanisms. *Pharmacol Res*. 2021;163:105224. doi:10.1016/j.phrs.2020.105224

48. Yu WY, Gao CX, Zhang HH, Wu YG, Yu CH. Herbal active ingredients: potential for the prevention and treatment of acute lung injury. *Biomed Res Int*. 2021;2021:5543185. doi:10.1155/2021/5543185

49. Chen H, Bai C, Wang X. The value of the lipopolysaccharide-induced acute lung injury model in respiratory medicine. *Expert Rev Respir Med*. 2010;4(6):773–783. doi:10.1586/ers.10.71

50. Qin L, Tan HL, Wang YG, et al. Astragalus membranaceus and Salvia miltiorrhiza ameliorate lipopolysaccharide-induced acute lung injury in rats by regulating the toll-like receptor 4/nuclear factor-kappa B signaling pathway. *Evid Based Complement Alternat Med*. 2018;2018:3017571. doi:10.1155/2018/3017571

51. Li Y, Jiang Y, Zhang H, et al. Research on acute lung injury inflammatory network. *Int J Clin Pharmacol Ther*. 2023;61(9):394–403. doi:10.5414/CP204438

52. Zhou H, Fan EK, Fan J. Cell-cell interaction mechanisms in acute lung injury. *Shock*. 2021;55(2):167–176. doi:10.1097/SHK.0000000000001598

53. Zhang Q, Yang C, Ma S, et al. Shiwei Qingwen decoction regulates TLR4/NF-κB signaling pathway and NLRP3 inflammasome to reduce inflammatory response in lipopolysaccharide-induced acute lung injury. *J Ethnopharmacol*. 2023;313:116615. doi:10.1016/j.jep.2023.116615

54. Deng G, He H, Chen Z, et al. Lianqinjiedu decoction attenuates LPS-induced inflammation and acute lung injury in rats via TLR4/NF-κB pathway. *Biomed Pharmacother*. 2017;96:148–152. doi:10.1016/j.biopha.2017.09.094

55. Hu X, Liu S, Zhu J, Ni H. Dachengqi decoction alleviates acute lung injury and inhibits inflammatory cytokines production through TLR4/NF-κB signaling pathway in vivo and in vitro. *J Cell Biochem*. 2019;120(6):8956–8964. doi:10.1002/jcb.27615

56. Patel VJ, Biswas Roy S, Mehta HJ, Joo M, Sadikot RT. Alternative and natural therapies for acute lung injury and acute respiratory distress syndrome. *Biomed Res Int*. 2018;2018:2476824. doi:10.1155/2018/2476824

57. Shi K, Xiao Y, Dong Y, et al. Protective effects of Atractylodis lancea Rhizoma on lipopolysaccharide-induced acute lung injury via TLR4/NF-κB and Keap1/Nrf2 signaling pathways in vitro and in vivo. *Int J Mol Sci*. 2022;23(24):16134. doi:10.3390/ijms232416134

58. Millar MW, Fazal F, Rahman A. Therapeutic targeting of NF-κB in acute lung injury: a double-edged sword. *Cells*. 2022;11(20):3317. doi:10.3390/cells11203317

59. Cross LJ, Matthay MA. Biomarkers in acute lung injury: insights into the pathogenesis of acute lung injury. *Crit Care Clin*. 2011;27(2):355–377. doi:10.1016/j.ccc.2010.12.005

60. Saikia S, Bordoloi M. Molecular docking: challenges, advances and its use in drug discovery perspective. *Curr Drug Targets*. 2019;20(5):501–521. doi:10.2174/1389450119666181022153016

61. Wang N, Geng C, Sun H, Wang X, Li F, Liu X. Hesperetin ameliorates lipopolysaccharide-induced acute lung injury in mice through regulating the TLR4-MyD88-NF-κB signaling pathway. *Arch Pharm Res*. 2019;42(12):1063–1070. doi:10.1007/s12272-019-01200-6

62. Changle Z, Cuiling F, Feng F, et al. Baicalin inhibits inflammation of lipopolysaccharide-induced acute lung injury toll like receptor-4/myeloid differentiation primary response 88/nuclear factor-kappa B signaling pathway. *J Tradit Chin Med*. 2022;42(2):200–212. doi:10.19852/j.cnki.jtcm.20211214.004

63. Han X, Ding W, Qu G, et al. Danshensu methyl ester attenuated LPS-induced acute lung injury by inhibiting TLR4/NF-κB pathway. *Respir Physiol Neurobiol*. 2024;322:104219. doi:10.1016/j.resp.2024.104219

64. Zhang A, Pan W, Lv J, Wu H. Protective effect of amygdalin on LPS-induced acute Lung injury by inhibiting NF-κB and NLRP3 signaling pathways. *Inflammation*. 2017;40(3):745–751. doi:10.1007/s10753-017-0518-4

65. Yeh CH, Yang JJ, Yang ML, Li YC, Kuan YH. Rutin decreases lipopolysaccharide-induced acute lung injury via inhibition of oxidative stress and the MAPK-NF-κB pathway. *Free Radic Biol Med*. 2014;69:249–257. doi:10.1016/j.freeradbiomed.2014.01.028

66. Zhao DH, Wu YJ, Liu ST, Liu RY. Salvianolic acid B attenuates lipopolysaccharide-induced acute lung injury in rats through inhibition of apoptosis, oxidative stress and inflammation. *Exp Ther Med*. 2017;14(1):759–764. doi:10.3892/etm.2017.4534

67. Yu W, Zeng M, Xu P, Liu J, Wang H. Effect of paeoniflorin on acute lung injury induced by influenza A virus in mice. Evidences of its mechanism of action. *Phytomedicine*. 2021;92:153724. doi:10.1016/j.phymed.2021.153724

68. Chu X, Ci X, He J, et al. Effects of a natural prolyl oligopeptidase inhibitor, rosmarinic acid, on lipopolysaccharide-induced acute lung injury in mice. *Molecules*. 2012;17(3):3586–3598. doi:10.3390/molecules17033586

69. Liu Q, Zhu CL, Li HR, et al. Salvianolic acid A protects against lipopolysaccharide-induced acute lung injury by inhibiting neutrophil NETosis. *Oxid Med Cell Longev*. 2022;2022:7411824. doi:10.1155/2022/7411824

70. Lv B, Guo J, Du Y, et al. Chlorogenic acid reduces inflammation by inhibiting the elevated expression of KAT2A to ameliorate lipopolysaccharide-induced acute lung injury. *Br J Pharmacol*. 2023;180(16):2156–2171. doi:10.1111/bph.16069

71. Tian C, Shao Y, Jin Z, et al. The protective effect of rutin against lipopolysaccharide induced acute lung injury in mice based on the pharmacokinetic and pharmacodynamic combination model. *J Pharm Biomed Anal*. 2022;209:114480. doi:10.1016/j.jpba.2021.114480